

# Coordination Control Between Excitation and Hydraulic System During Mode Conversion of Variable Speed Pumped Storage Unit

Yahong Chen<sup>✉</sup>, Changhong Deng, and Yating Zhao

**Abstract**—Variable speed pumped storage (VSPS) unit has various operation modes and it is often required by the dispatcher to convert rapidly and frequently between these modes. Unlike conventional units, however, VSPS is controlled by both excitation and hydraulic system, and control of them is independent of each other. The mismatch between the rapid electromagnetic response of the former and the relatively slow mechanical response of the latter could result in unfavorable transients or even conversion failure. Hence, coordination controls between excitation and hydraulic system during mode conversion is a meaningful topic but has seldom been investigated. To this end, the electromechanical transient model of VSPS considering the excitation dynamics of the converter is first established. Then, a multistage soft coordination control strategy is proposed in this article. By applying this strategy, the soft and smooth mode conversion of VSPS is achieved with favorable dynamic performances during the complete conversion process. And finally, simulation and experimental results verified the effectiveness of the strategy.

**Index Terms**—Coordination control, excitation system, hydraulic system, mode conversion, variable speed pumped storage (VSPS).

## NOMENCLATURE

$H_g$	Inertia time constant of doubly fed induction machine (DFIM).	$u_g$	Voltage of grid.
$H_t$	Inertia time constant of reversible pump turbine (RPT).	$u_s$	Voltage of stator for DFIM.
$D_g$	Damping coefficient of DFIM.	$R_s$	Resistance of stator for DFIM.
$\alpha$	Speed ratio between RPT and DFIM.	$R_r$	Resistance of rotor for DFIM.
$u_{ds}, u_{qs}, i_{ds}, i_{qs}, \psi_{ds}, \psi_{qs}$	Voltage, current, and flux of stator.	$\psi_s$	Stator flux of DFIM.
$u_{dr}, u_{qr}, i_{dr}, i_{qr}, \psi_{dr}, \psi_{qr}$	Voltage, current, and flux of rotor.	$L_m$	Mutual-inductance between stator and rotor.
$s$	Slip ratio of DFIM.	$L_s$	Self-inductance of stator.
$d, q, 0$	Components of $d$ -axis, $q$ -axis and 0 axis.	$L_r$	Self-inductance of rotor.
		$V_{dc}$	DC bus voltage of converter.
		$T_{rc}$	Time constant of excitation response.
		$k_p, k_i, k_d$	Control coefficients of speed governor.
		$T_{1v}$	Time constant of differential decay.
		$k_a, t_a$	Response coefficients of actuator.
		$\theta_g$	Phase of grid voltage.
		$\theta_s$	Phase of stator voltage.
		$\theta_{Trans}$	Angle for the transformation of coordinates.
		$\theta_{g\_rad}$	Angle of grid voltage.
		$\theta_{r\_rad}$	Angle of the rotor.
		$\theta_f$	Angle of excitation current.
		$\theta_\psi$	Angle of the magnetic field.
		$\theta_c$	Angle for compensation.
		$K_p, K_i, K_d$	Parameters of phase compensation controller.
		$T_m$	Input mechanical torque of RPT.
		$T_t$	Output mechanical torque of RPT.
		$T_e$	Electromagnetic torque of DFIM.
		$\omega_r$	Angular velocity of the rotor.
		$\omega_f$	Angular velocity of rotor excitation current.
		$\omega_g$	Angular velocity of grid voltage.
		$\omega_s$	Angular velocity of stator voltage.
		$\omega_{ref}$	Reference speed of rotor.
		$\Delta\omega_{set}$	Set value of the increment of speed.
		$T_{cmd}$	Instruction of torque for VSPS.
		$P_{cmd}$	Instruction of active power for VSPS.
		$\omega_{opt}$	Optimal speed of VSPS.
		$y_{opt}$	Optimal guide vane opening.
		$y$	Electrical instruction of guide vane opening.

Manuscript received September 10, 2020; revised November 24, 2020 and January 10, 2021; accepted February 15, 2021. Date of publication February 23, 2021; date of current version June 1, 2021. This work was supported by The National Key Research and Development Program of China under Grant 2017YFB0903705. Recommended for publication by Associate Editor Y. A.-R. I. Mohamed. (*Corresponding author: Changhong Deng*.)

The authors are with the School of Electrical Engineering and Automation, Wuhan University, Wuhan 430072, China (e-mail: 992398662@qq.com; dengch@whu.edu.cn; yatingzhao63@gmail.com).

Color versions of one or more figures in this article are available at <https://doi.org/10.1109/TPEL.2021.3061268>.

Digital Object Identifier 10.1109/TPEL.2021.3061268

$Y$	Mechanical position of guide vane opening.
$T_{1v}$	Time constant of decay.
$Q_{cmd}$	Set-point of reactive power.
$H_s$	Static head.
$h_w$	Constant of pipeline characteristic.
$T_w$	Time constant of water hammer.
$T_r$	Time constant of water reflection.
$t_{up}$	Setting time for load increase.
$t_{dow}$	Setting time for load rejection.
$T_{up}$	Target value of torque.
$\omega_{rc}$	Cutoff angular frequency of quasi-proportional resonance controller (QPRC).
$\omega_{rr}$	Resonant angular frequency of QPRC.
$f_0(t), f_1(t)$	Elements of the switching control function.
$y_{0-}$	The final state of the signal being replaced.
$y_1(t)$	The signal being put in.
$p$	Differential operator.
$R^+$	Positive real number.

## I. INTRODUCTION

THE variable speed pumped storage (VSPS) unit has become increasingly popular in the modern power grid due to its improved hydraulic efficiency over the wide head range and rapid power controllability [1], [2].

VSPS has a variety of operating modes (in turbine or pump condition) [3], such as static mode, startup mode, steady-state mode, synchronous condenser, and shutdown mode, etc. Typically, it is often required by the system dispatchers that VSPS can switch frequently and rapidly between these modes, depending on the needs of the grid.

However, due to the weak coupling between the excitation system (composed of a doubly fed induction machine (DFIM) and a back-to-back converter) and hydraulic system (composed of a speed governor and a reversible pump-turbine (RPT)), mode conversion control of VSPS is becoming more complicated. Besides, the response speed of the former is fairly fast with a time scale of tens of milliseconds, while the latter is relatively slow with a time scale of seconds. If there is no proper coordination between the two systems, the mismatch in response speeds between them could result in conversion failure or even operation instability of VSPS [4], [5].

For mode conversion control of VSPS, a few pieces of research have been reported. In [6], a volts/hertz (V/f) smooth starting and regenerative braking strategy is proposed. In [7], a model predictive control based closed-loop self-starting and synchronization strategy of VSPS is presented. In [8], the dynamics of VSPS with the quaternary configuration at multiple operation modes are investigated.

However, these literatures only focus on the control of a single-stage during mode conversion, while neglecting the

smooth and cohesive transition control methods between stages. This is likely to produce current or torque impacts on the unit or even result in the unit losing control on rotor speed during the transition between stages. Therefore, research on the coordination control during the whole stages of mode conversion is meaningful, but still lacking yet.

Summarize the existing literatures related to VSPS, researches are mainly divided into the following areas: mode control on a single stage, modeling methods [2], [9], dynamic response analysis [4], stability analysis [10], fault ride-through [11], protection [12], converter excitation control [5], and operation optimization [13], etc. How to coordinate the excitation system and hydraulic system with response speed nearly 1000 times different is challenging but has not been investigated till now.

The modeling of VSPS is an important task. Schmidt *et al.* [14] developed a comprehensive model of VSPS, which laid special emphasis on the accurate description of water hammer effects. Nevertheless, the focus of this article is on the coordinate methods between excitation and hydraulic system during mode conversion, the detailed and over-complex model of VSPS is not only unnecessary but also brings a high computational burden; hence, a proper simplification of the model is necessary [13]. Pannatier *et al.* [13] proposed a pseudo-continuous model of the converters feeding the rotor circuits of VSPS, and Sarasúa *et al.* [15] demonstrated a linearized reduced order dynamic model of VSPS. These models have been proved to be effective in reducing system complexity. However, the excitation dynamics of the converter are neglected.

In this article, the simplified electromechanical transient model of VSPS, in turbine mode, is established as a supplement to the existing models. Then a multistage soft coordination control (SCC) strategy is proposed. The strategy is divided into three main stages, namely soft cut-in control, steady-state operation, and soft cut-out control. By applying this strategy, the problem of how to coordinate the control between the excitation system and the hydraulic system, to prevent conversion failure of VSPS, is solved. In the strategy, the smooth transition between stages and the excitation dynamics of the converter are considered as well.

The main contributions are as follows.

- 1) The coordination control strategy endows VSPS with the ability to rapidly complete the process of mode conversion, thus the unit has the advantage of being capable to fast respond to operator commands in an emergency.
- 2) The strategy enables VSPS to repeatedly cut in and out of the grid with minimum impacts on the grid and the unit itself.
- 3) The architecture provides VSPS capabilities to smoothly and softly convert from one mode to another, and synchronize with the grid during variable speed conditions.
- 4) The overall control strategy is quite simple and convenient for practical applications and has not been presented before.

The rest of this article is organized as follows. Section II presents the simplified electromechanical transient model of

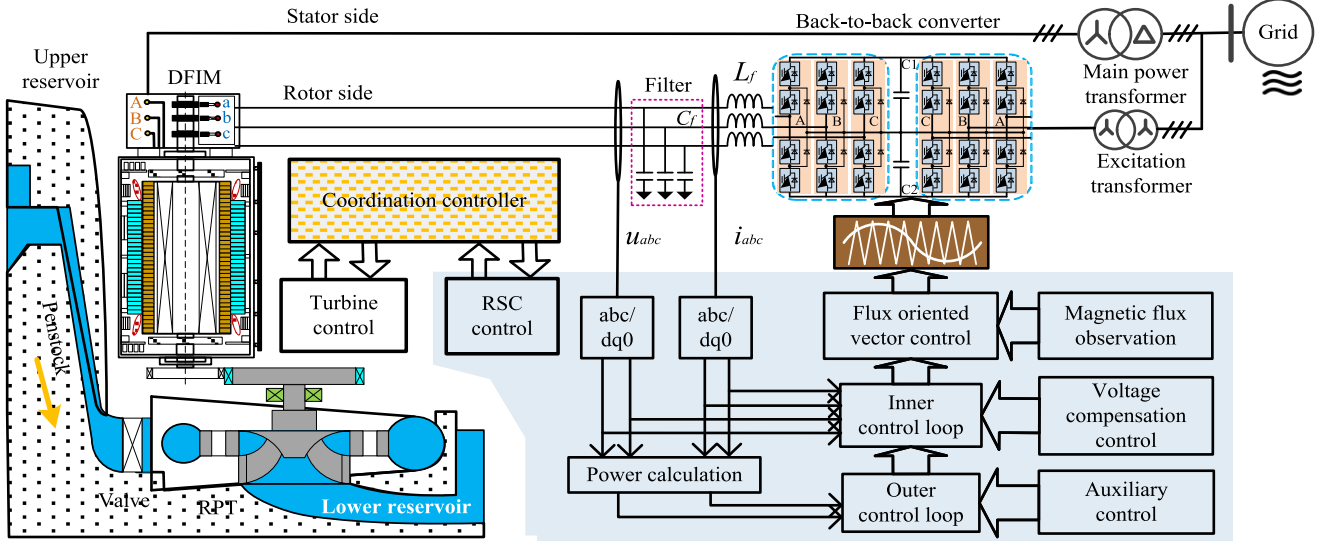


Fig. 1. Overall control diagram of VSPS.

VSPS. Sections III–V present the coordination control strategy. The simulation and experimental results are demonstrated in Sections VI and VII, respectively. Finally, conclusions are drawn in Section VIII.

## II. ELECTROMECHANICAL TRANSIENT MODEL OF VSPS

VSPS is mainly composed of the penstock, RPT, speed governor, DFIM, back-to-back converter and its control system, and coordination controller [4], [13], as shown in Fig. 1.

### A. Model of DFIM-Converter System

The 5th-order dynamic model with electromagnetic transient processes, as presented in [9], is adopted by DFIM. This model uses five-state variables, with four for the electromagnetic dynamics (fluxes linkages and induced voltages associated with the main field winding and damper windings) and one for the rotor mechanical motion (rotor speed). The model of DFIM has been introduced in a vast number of literatures and will not be repeated in this manuscript.

The back-to-back converter is responsible for providing three-phase alternating excitation current to DFIM. Through adjusting the amplitude, frequency, and phase of excitation current, power (or torque) and speed of DFIM can be directly controlled. As a supplement to the widely used models of vector control and decouple control [2], [9], the dynamics of excitation frequency regulation of converter is given as follows:

$$T_{rc} \frac{d\omega_f}{dt} = \omega_s - (\omega_r + \omega_f) \quad (1)$$

$$\begin{aligned} \frac{d\theta_\psi}{dt} &= \omega_r + \omega_f, \theta_\psi = \theta_{r\_rad} + \theta_f, \theta_{r\_rad} \\ &= \omega_r t, \theta_f = \omega_f t. \end{aligned} \quad (2)$$

In steady state,  $\omega_r + \omega_f = \omega_s$ .

### B. Model of RPT-Water Conveyance System

The model of RPT describes the relationship between guide vane opening (GVO) and output mechanical torque. When GVO changes the flow and torque of RPT would change accordingly. The change of flow rate causes the change of pressure in the water conveyance system, and the change of water pressure in turn causes the change of turbine torque and flow rate. For the type of mixed-flow turbine, in the case that the speed range is not wide, the impact of the speed on the flow can be ignored, that is  $e_{qw} \approx 0$ . In addition, the self-regulating coefficient of RPT  $e_{T\omega}$  is often combined with the self-regulating coefficient of the load in the rotor motion equation model of the generator. Therefore, the dynamic model of RPT is given as follows [2], [16]:

$$G_t(s) = \frac{T_m(s)}{Y(s)} = \frac{e_{Ty} - (e_{Ty}e_{qh} - e_{Th}e_{qy})G_h(s)}{1 - e_{qh}G_h(s)}. \quad (3)$$

Considering the dynamics of water flow caused by the compressibility of water and elasticity of penstock, the nonlinear elastic water hammer model is given as follows [16]:

$$G_h(s) = \frac{\Delta h(s)}{\Delta q(s)} = -2h_w \frac{e^{\frac{T_r}{2}s} - e^{-\frac{T_r}{2}s}}{e^{\frac{T_r}{2}s} + e^{-\frac{T_r}{2}s}}. \quad (4)$$

For short penstock (within 600–800 m), the nonlinear model can be simplified as a rigid water hammer model [2], as follows:

$$G_h(s) = \frac{\Delta h(s)}{\Delta q(s)} = -T_w s \quad (5)$$

where  $e_{Ty}$ ,  $e_{T\omega}$ ,  $e_{Th}$ ,  $e_{qy}$ ,  $e_{q\omega}$ , and  $e_{qh}$  are the transfer coefficients of RPT,  $h$  is the dynamic head, and  $q$  is the dynamic flow rate.

### C. Model of Rotor Motion

Considering the torque increment  $(\partial T / \partial \omega_r) \Delta \omega_r = e_{T\omega} \Delta \omega_r$  which is caused by the increment of rotating speed, the rotor

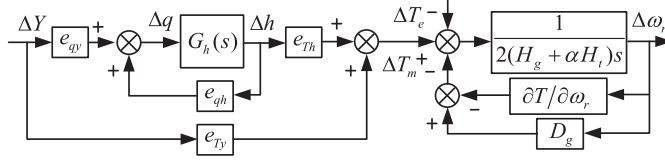


Fig. 2. Dynamic model of RPT-generator system.

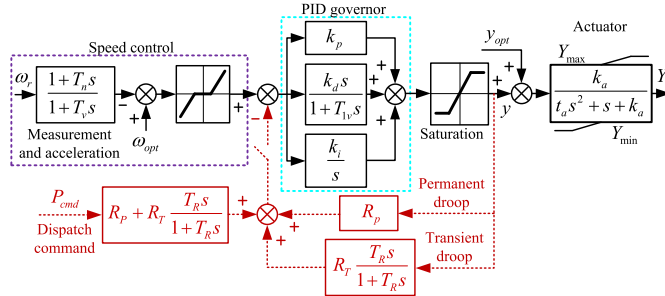


Fig. 3. Dynamic model of a speed governor.

motion equation of RPT is obtained as follows:

$$2\alpha H_t \frac{d\omega_r}{dt} = T_m - T_t + \frac{\partial T}{\partial \omega_r} \Delta \omega_r. \quad (6)$$

The rotor motion equation of DFIM [9] is given as follows:

$$2H_g \frac{d\omega_r}{dt} = T_t - T_e - D_g \Delta \omega_r. \quad (7)$$

Combine (7) with (6), after Laplace transformation the rotor motion equation of the RPT-Generator system is obtained

$$G(s) = \frac{\Delta \omega_r(s)}{\Delta T(s)} = \frac{1}{2(H_g + \alpha H_t)s + D_g - \partial T / \partial \omega_r}. \quad (8)$$

The dynamic model of the RPT-Generator system considering the water hammer effect is shown in Fig. 2, where  $e_{Ty}$ ,  $e_{Tw}$ ,  $e_{Th}$ ,  $e_{qy}$ ,  $e_{q\omega}$ , and  $e_{qh}$  are transfer coefficients of RPT.

#### D. Model of Speed Governor

The speed governor is mainly composed of a PID controller and electro-hydraulic servo actuator, as shown in Fig. 3. The main function of the PID controller is to adjust the reference value of GVO dynamically according to the speed deviation of VSPS. The model of the PID controller is expressed as follows:

$$y(s) = \left( k_p + \frac{k_i}{s} + \frac{k_d s}{1+T_{1v}s} \right) [\omega_r(s) - \omega_{opt}(s)]. \quad (9)$$

The function of the actuator is to convert the electrical signal given by the PID controller into mechanical position of the guide blade, thus affecting the output mechanical torque of RPT and forcing the speed of the rotor to track its reference value. The transfer function of the actuator is given as follows:

$$G_1(s) = \frac{Y(s)}{y(s)} = \frac{k_a}{t_a s^2 + s + k_a}. \quad (10)$$

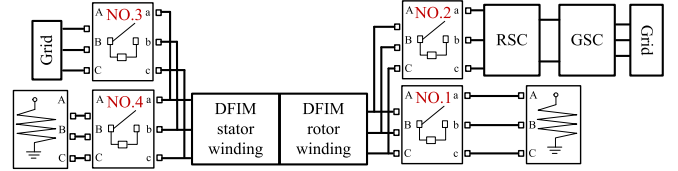


Fig. 4 Configuration of the circuit breaker.

### III. STAGE OF SOFT CUT-IN CONTROL OF VSPS

#### A. Stage of Soft Self-Starting

If VSPS received the startup command and is required to cut-in grid, NO.1 and NO.4 short-circuit breakers (see Fig. 4) for stator and rotor windings of DFIM are closed, and the PWM signals of the converter are blocked, both by the coordination controller. Hence, the electromagnetic torque of DFIM  $T_{em} = 0$ . Then speed governor gradually adjust GVO to the no-load opening value. The output mechanical torque  $T_m$  of RPT consequently increases gradually, and the speed of the rotor is driven to accelerate. The starting process is completed when the rotor is accelerated to around the synchronous speed.

In the process, the reference value  $\omega_{ref}$  of speed governor is increased dynamically with the speed  $\omega_r$ , given as follows:

$$\omega_{ref}(t) = \omega_r(t) + \Delta \omega_{set}, t \in R^+. \quad (11)$$

During the acceleration stage of VSPS, the value of  $\Delta \omega_{set}$  is constant. Ignoring the dynamics of guide vane and RPT, the speed of the rotor can be obtained

$$\omega_r(t) = \frac{\Delta \omega_{set}}{2(H_g + \alpha H_t)} [(k_p - D_g + \partial T / \partial \omega_r)t + \frac{k_i}{2} t^2] \\ k_p > D_g - \partial T / \partial \omega_r, t \in R^+. \quad (12)$$

Parameters of the speed governor are the dominant factors in determining the no-load acceleration process of VSPS. In general,  $k_d = 0$ , so there is no differential item here. The value of  $k_p$  must satisfy  $k_p > D$ , otherwise, the rotation speed will be reversed. The value of  $k_i$  can determine the acceleration speed of the rotor. Since in general  $k_i \ll k_p$ , the above equation can be further simplified as

$$\omega_r(t) = \Delta \omega_{set} \frac{k_p - D_g + \partial T / \partial \omega_r}{2(H_g + \alpha H_t)} t \\ k_p > D_g - \partial T / \partial \omega_r, t \in R^+. \quad (13)$$

The speed of acceleration (or torque of RPT) can be adjusted by the value of  $\Delta \omega_{set}$  and the speed of the rotor is increased at an approximately constant speed.

#### B. Stage of Terminal Voltage Control

Due to the large capacity of VSPS (hundreds of megawatt) and the small leakage impedance of the stator, if there is a small voltage or phase difference between the stator and grid, a great destructive impulse current will be produced. Hence, a two-stage soft cut-in control strategy is proposed to minimize the impulse current at the instance of cut-in, where establishing

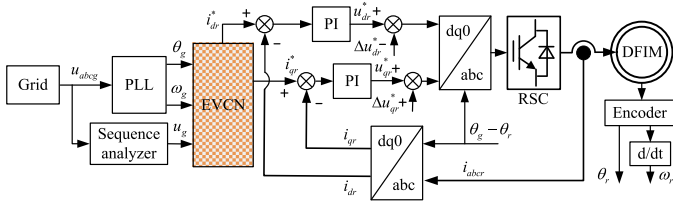


Fig. 5. Diagram of EVCN control.

voltage control under no-load (EVCN) is the first stage of the strategy, and voltage compensation control (VCC) is the second stage, as elaborated below.

1) *EVCN Control*: The voltage of the stator must be established before the stator is connected to the grid. The prominent feature of the proposed EVCN method is that the current of the stator is zero before grid-connection. Thus, the order of the DFIM model can be reduced and the control algorithm can be simplified [18].

The control process of EVCN is as follows. First, after the rotor being accelerated to around the synchronous speed, NO.1 and NO.4 short circuit breakers are tripped and NO.2 breaker is closed, then the excitation control system is put into operation (the control signals are sent successively by the coordination controller according to the control logic). Second, the converter controller calculates the space vector of stator flux  $\psi_s$  according to the information of grid voltage (amplitude, frequency, and phase), and conducts excitation control on the rotor. Third, the voltage of the stator is gradually established. The block diagram of EVCN is shown in Fig. 5.

Since the current of the stator is zero under no-load,  $i_{ds} = i_{qs} = 0$  can be obtained. According to [9], the model of DFIM under no-load can be derived as follows.

Voltage equations of stator and rotor under no-load

$$\begin{cases} u_{ds} = -p\psi_{ds} + \omega_s\psi_{qs} \\ u_{qs} = -p\psi_{qs} - \omega_s\psi_{ds} \\ u_{dr} = R_r i_{dr} + p\psi_{dr} - s\omega_s\psi_{qr} \\ u_{qr} = R_r i_{qr} + p\psi_{qr} + s\omega_s\psi_{dr}. \end{cases} \quad (14)$$

Flux equations of stator and rotor under no-load

$$\begin{cases} \psi_{ds} = -L_m i_{dr} \\ \psi_{qs} = -L_m i_{qr} \\ \psi_{dr} = L_r i_{dr} \\ \psi_{qr} = L_r i_{qr}. \end{cases} \quad (15)$$

Applying the field-oriented vector control method, and orient  $d$ -axis of dq0 frame along the direction of  $\psi_s$ , then  $\psi_{ds} = |\psi_s|$  and  $\psi_{qs} = 0$  are obtained. Based on the model of DFIM under no-load, and considering the orientation error and the cross-coupling between  $d$ -axis and  $q$ -axis of rotor current, the control voltage of the outer loop of the converter is obtained

$$\begin{cases} u_{dr}^* = (R_r + L_r p) i_{dr}^{*EVCN} \\ u_{qr}^* = (R_r + L_r p) i_{qr}^{*EVCN} \end{cases} \quad (16)$$

$$\begin{cases} i_{dr}^{*EVCN} = \frac{-|\psi_s|}{L_m}, |\psi_s| = \frac{u_g}{\omega_g} \\ i_{qr}^{*EVCN} = 0. \end{cases} \quad (17)$$

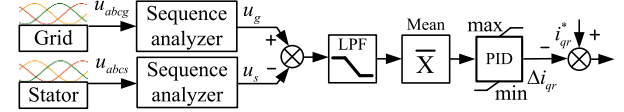


Fig. 6. Diagram of voltage amplitude compensation control.

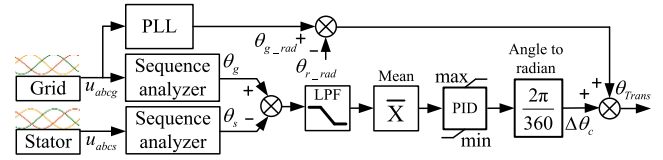


Fig. 7. Diagram of direct phase compensation control.

The compensation voltage of the inner loop of converter is

$$\begin{cases} \Delta u_{dr}^{EVCN} = -(\omega_g - \omega_r) L_r i_{qr}^{*EVCN} \\ \Delta u_{qr}^{EVCN} = (\omega_g - \omega_r) L_r i_{dr}^{*EVCN}. \end{cases} \quad (18)$$

The control voltage of the converter can be written as

$$\begin{cases} u_{dr} = u_{dr}^* + \Delta u_{dr}^{EVCN} \\ u_{qr} = u_{qr}^* + \Delta u_{qr}^{EVCN}. \end{cases} \quad (19)$$

2) *VCC Compensation Control*: After the voltage of VSPS is established, it fails to meet the requirements of quasi-synchronous grid-connection (the amplitude difference, frequency difference, and phase difference between stator and grid are demanded to less than the threshold values). VCC control is thus employed to adjust the voltage of the stator, by changing the excitation current.

a) *Voltage Amplitude Compensation Control*: The essence of EVCN control is the open-loop control of voltage. In the actual grid-connection process, there is generally a voltage amplitude difference between stator and grid due to sampling errors of voltage and current, and variation of DFIM parameters. Because of the defect that the steady-state accuracy of open-loop voltage control is insufficient, the closed-loop VCC is carried out to improve the voltage amplitude tracking accuracy of the stator with grid, as shown in Fig. 6

$$\Delta i_{qr} = \left( K_p + \frac{K_i}{s} + K_d s \right) (u_g - u_s). \quad (20)$$

b) *Direct Phase Compensation Control*: Affected by the orientation accuracy of the dq0 frame, variation of parameters, the error of measurements, and other random factors, there is a phase difference between stator and grid. A direct phase compensation control method is proposed, as shown in Fig. 7. The compensation angle  $\Delta\theta_c$  is formed by the controller by applying this method according to the phase difference between the stator and grid. And then, the controller directly changes the phase of the excitation current of the rotor so that the phase of the stator remains consistent with the grid.

The compensation angle  $\Delta\theta_c$  is calculated as follows:

$$\Delta\theta_c = \left( K_p + \frac{K_i}{s} + K_d s \right) (\theta_g - \theta_s). \quad (21)$$

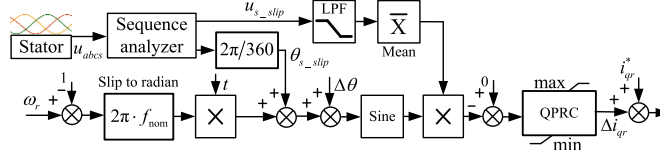


Fig. 8. Diagram of voltage fluctuation compensation control.

The angle of position used for coordinate transformation of rotor excitation current is given as follows:

$$\theta_{Trans} = \theta_{g\_rad} - \theta_{r\_rad} + \Delta\theta_c. \quad (22)$$

c) *Slip Frequency Fluctuation Compensation Control*: Influenced by the ripple in dc bus voltage of the converter, the inconsistent characteristics of power devices, and the truncation error of A/D sampling, the output of the converter often contains a dc component, which in turn causes the voltage of the stator to fluctuate at slip frequency through electromagnetic induction. However, due to the poor tracking performance of the PID controller to the ac signal, the controller cannot be used to eliminate the slip frequency voltage fluctuation, and could even amplify the low-frequency noises.

To solve this problem, a quasi-proportional resonance controller (QPRC) is used to compensate for the voltage so that a band with a large gain near the slip resonance frequency is formed at the amplitude-frequency curve of the controller. Thus, the controller can track and eliminate the fluctuation of stator voltage at slip frequency accurately, as shown in Fig. 8.

The transfer function of QPRC is given as follows:

$$G_{QPRC}(s) = K_P + \frac{2\omega_{rc}K_I s}{s^2 + 2\omega_{rc}s + \omega_{rr}^2}. \quad (23)$$

After applying VCC control, when all the requirements are satisfied, the NO.3 circuit breaker closes and the process of grid-connection is completed. For the reason that the voltage of the stator is strictly synchronized with the grid before closing the breaker, the impulse current produced at the instant of grid-connection is very weak. VSPS can be connected to the grid without impact in the process of speed fluctuation.

### C. Stage of Soft Mode-Switching Control

The current of the stator is zero before grid-connection while not after connection. Hence, the status of DFIM, converter, and control systems are quite different before and after connection. Besides, the converter works in EVCN mode before connection while in PQ control (PQC) mode, which enables VSPS to output the specified active and reactive power, after connection. Consequently, the first thing that needs to be done by the controller of the converter is the switch of control mode after VSPS is successfully connected to the grid.

Direct and hard switch of control mode will cause a sudden change of the status of the control system and excitation voltage of the rotor, which will lead to failure of the mode switch of the converter, or oscillation of voltage, current, and power of VSPS [19]. In order to guarantee the continuity of status of the outer

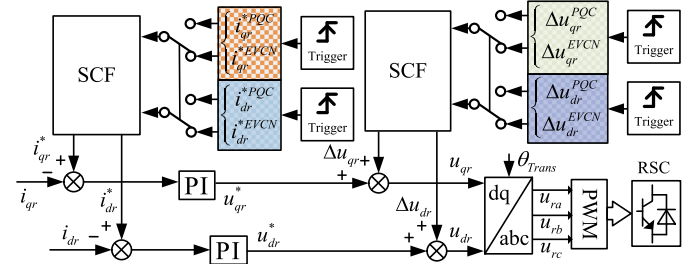


Fig. 9. Diagram of soft mode-switching control.

and inner control loops of the converter before and after mode switch, and to make excitation voltage and current of the rotor smoothly transit to the new status, a soft mode-switching control strategy is proposed, as shown in Fig. 9.

The switching control function (SCF) is given as follows:

$$y(t) = f_0(t)y_{0-} + f_1(t)y_1(t), t \in \left[0, \frac{1}{k}\right], k \in R^+ \quad (24)$$

$$\begin{cases} f_0(t) = 1 - kt, & t \in [0, \frac{1}{k}], k \in R^+. \\ f_1(t) = kt \end{cases} \quad (25)$$

### D. Stage of Soft Load Increasing Control

After mode switching is completed, the power of VSPS must first be adjusted above the minimum allowable value to prepare the unit to provide frequency control service for the grid.

Since the power of VSPS is directly controlled by the converter while the speed is controlled by the speed governor, the sudden change of power will inevitably lead to the fluctuation of speed. And, the higher the rate of power change, the greater the degree of rotation speed fluctuation. To avoid the excessive fluctuation of speed, which would lead to the intensification of turbine vibration and the increase of cavitation coefficient, the reference value of converter is linearly increased to the target value at a limited rate

$$T_{cmd} = T_{up} \frac{1}{t_{up}} t, t \in [0, t_{up}], t_{up} \in R^+. \quad (26)$$

## IV. STAGE OF STEADY-STATE OPERATION OF VSPS

### A. Optimization of Speed and GVO

VSPS has the highest efficiency at the rated head with rated load. The operation efficiency decreases when the static head and required output power change. The highest hydraulic efficiency of VSPS can be achieved utilizing speed optimization and GVO optimization, according to the comprehensive operation characteristics of RPT [4], [13]. The linearly approximated optimal speed and optimal GVO are demonstrated in Fig. 10, and the corresponding equations are expressed as follows [17]:

$$\omega_{opt}(P_{cmd}, H_s) = 0.95 + 1.25(P_{cmd} - 0.8) - 0.25(H_s - 0.8) \quad (27)$$

$$y_{opt}(P_{cmd}, H_s) = 0.8 + P_{cmd} - H_s. \quad (28)$$

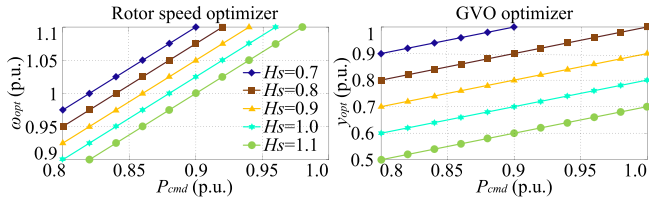
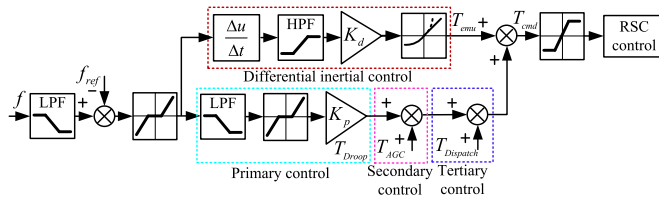
Fig. 10. Relation of optimal speed and GVO with  $P_{cmd}$  and  $H_s$ .

Fig. 11. Loop of automatic frequency control.

### B. Control Strategy

At this stage, VSPS operates in PQC mode, and the converter directly controls the active and reactive power of the unit. Since most of the time VSPS operates at this stage, the highest hydraulic efficiency of the unit can be achieved thus improving the economic benefit of operation, through the optimization of speed and GVO and the coordination between converter and speed governor. In addition to that, when the frequency of the power system changes, the control function of the outer loop of the converter enables VSPS to automatically participate in frequency regulation of the system (for instance, primary frequency regulation and virtual inertia control), so as to assist in stabilizing the system frequency, as shown in Fig. 11.

The relation between the current reference of the rotor and power reference of VSPS is given as follows:

$$\begin{cases} i_{qr}^{*PQC} = \frac{2L_s\omega_r}{3L_m u_s} T_{cmd} \\ i_{dr}^{*PQC} = \frac{\psi_s}{L_m} + \frac{2L_s}{3L_m u_s} Q_{cmd}. \end{cases} \quad (29)$$

The compensation voltage for decoupling control of the converter is given as follows [20]:

$$\begin{cases} \Delta u_{dr}^{PQC} = R_r i_{dr}^{*PQC} - (\omega_s - \omega_r)(L_r i_{qr}^{*PQC} + L_m i_{qs\_estim}) \\ \Delta u_{qr}^{PQC} = R_r i_{qr}^{*PQC} + (\omega_s - \omega_r)(L_r i_{dr}^{*PQC} + L_m i_{ds\_estim}) \end{cases} \quad (30)$$

$$\begin{cases} i_{ds\_estim} = \frac{R_s}{\omega_s^2 L_s^2 + R_s^2} (V_{dc} - \frac{\omega_s^2 L_m L_s}{R_s} i_{dr}^{*PQC} + \omega_s L_m i_{qr}^{*PQC}) \\ i_{qs\_estim} = -\frac{\omega_s L_s}{R_s} i_{ds\_estim} - \frac{\omega_s L_m}{R_s} i_{dr}^{*PQC}. \end{cases} \quad (31)$$

### V. STAGE OF SOFT CUT-OUT CONTROL OF VSPS

When it is commanded to shutdown VSPS or to switch to pump mode, it is necessary to carry out cut-out control and disconnect the unit from the grid. Soft cut-out control requires that stator current of the unit close to zero at the instant of

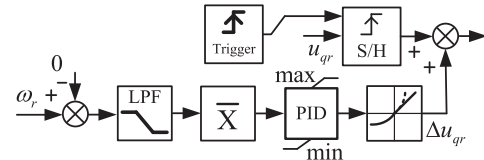


Fig. 12. Diagram of regenerative braking.

disconnection, and the control process is divided into three stages as follows.

#### A. Stage of Soft Load Rejection Control

After VSPS received load rejection instruction, the power of the unit should decrease to zero gradually. To avoid the drastic fluctuation of rotation speed or system frequency resulted from the sudden change of unit power, the reference value of the converter is linearly decreased to zero at a limited rate

$$T_{cmd} = T_{em\_0-} \left( 1 - \frac{1}{t_{dow}} t \right), t \in [0, t_{dow}], t_{dow} \in R^+. \quad (32)$$

#### B. Stage of Regenerative Braking Control

After the power (or stator current) of VSPS is reduced to zero, the guide vane is rapidly closed and the converter is switched from PQC mode to closed-loop speed control mode. By applying the control algorithm (see Fig. 12), VSPS is enabled to feedback its rotational energy to the grid. With the action of mechanical damping and electromagnetic damping, the speed of VSPS drops to zero rapidly.

#### C. Stage of Disconnection Control

When the speed of VSPS is reduced to zero, the tripping signal of NO.3 breaker is given. After the action of the breaker, VSPS is disconnected with the grid under zero stator current thus soft cut-out control of the unit is realized.

The complete flowchart of the proposed multistage SCC is as shown in Fig. 13.

## VI. SIMULATION RESULTS

The simulation results of the proposed SCC coordination control strategy applied at each stage of mode conversion of VSPS, i.e., from startup to shut-down, are demonstrated. Due to the space limitation, only results of VSPS in turbine condition are included. The parameters of VSPS and control parameters used in the simulation are given in Tables I–III and the Appendix, respectively. Note that, the parameter values without indicating the unit represents the unit value.

#### A. Results of Cut-In Control

Fig. 14 demonstrates the results of self-starting when the reference value of speed governor  $\omega_{ref}$  takes  $\omega_{opt}$  and  $\Delta\omega_{set}$  ( $\Delta\omega_{set} = 0.4, 0.17$ , and  $0.05$ ) respectively. It can be seen that, the degree of reverse adjustment of torque are  $\delta_1 = 0.12$ ,  $\delta_2 =$

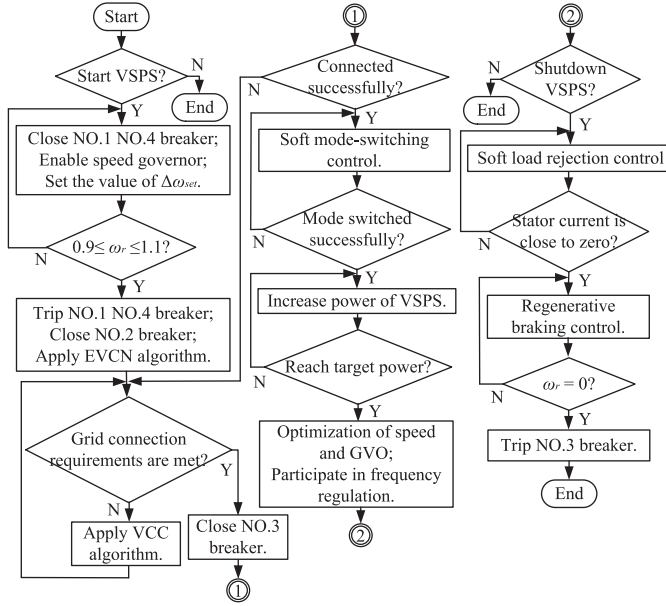


Fig. 13. Flowchart of proposed multistage SCC.

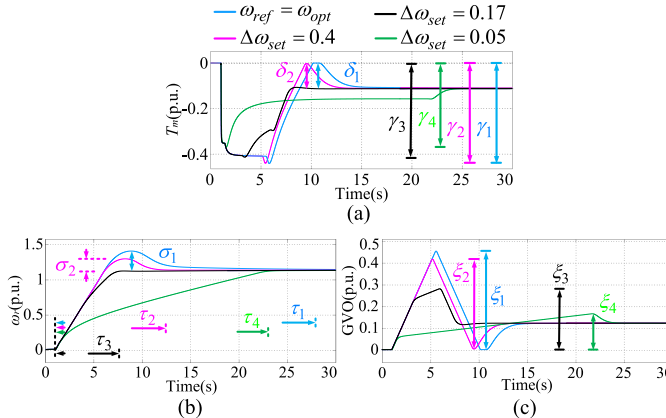


Fig. 14. Results of soft self-starting. (a) Mechanical torque. (b) Speed of rotor. (c) GVO.

0.12,  $\delta_3 = 0$ , and  $\delta_4 = 0$ . The maximum torque variation are  $\gamma_1 = 0.44$ ,  $\gamma_2 = 0.44$ ,  $\gamma_3 = 0.42$ , and  $\gamma_4 = 0.38$ . The overshoot are  $\sigma_1 = 27\%$ ,  $\sigma_2 = 18\%$ ,  $\sigma_3 = 0$ , and  $\sigma_4 = 0$ . The settle time are  $\tau_1 = 28s$ ,  $\tau_2 = 12.5s$ ,  $\tau_3 = 7.6s$ , and  $\tau_4 = 23s$ . And, the maximum GVO variation are  $\xi_1 = 0.45$ ,  $\xi_2 = 0.42$ ,  $\xi_3 = 0.28$ , and  $\xi_4 = 0.17$ . It clearly shows that, if  $\omega_{ref} = \omega_{opt}$ , not only the fluctuation degree of GVO and mechanical torque is the largest, but also the overshoot of speed is the biggest, and the time needed to stabilize the rotor is the longest. However, by adopting the proposed soft self-starting strategy and taking the appropriate value of, for instance, 0.17, not only the fluctuation degree of GVO and mechanical torque can be significantly reduced, but also the time for the rotor to reach steady-state is the shortest. These control effects cannot be achieved at the same time by the traditional method of adjusting parameters of the PID controller. Thus, the advantages of the self-starting strategy proposed in this manuscript in controlling the speed of VSPS are proved.

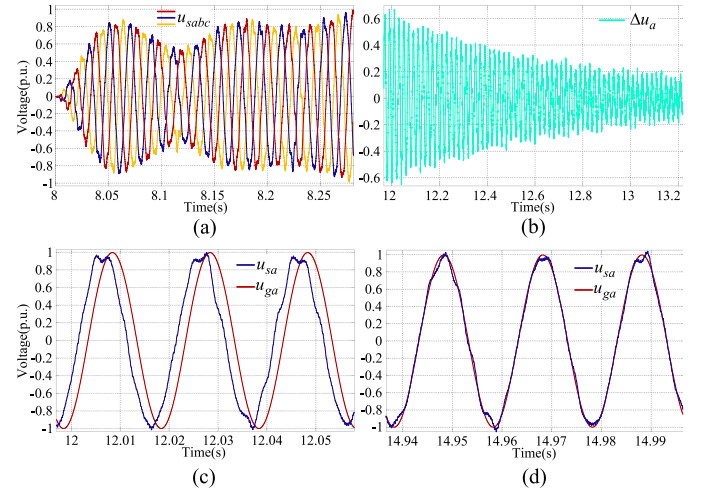


Fig. 15. Comparison of voltage. (a) Voltage of stator. (b) Voltage difference between grid and stator. (c) Contrast of phase at initial stage. (d) Contrast of phase at late stage.

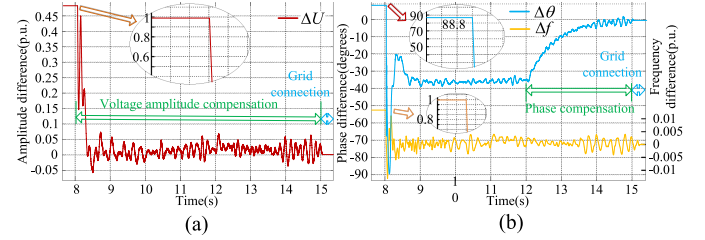


Fig. 16. Effects of SCC control. (a) Amplitude difference. (b) Frequency and phase difference.

It is shown in Fig. 15(a) that, the voltage of VSPS was established in a very short time (within 0.3 s) by using the SCC control algorithm. Meanwhile, it can be observed from Fig. 15(b) to (d) that the waveform of stator voltage converges to that of the grid rapidly, and the voltage difference between them becomes smaller and smaller from 12 s through SCC control, which proves the effectiveness of the strategy.

It is demonstrated in Fig. 16 that, after applying the amplitude compensation control strategy, which starts from 8 s, the voltage amplitude error difference between stator and grid is then controlled within  $\pm 0.07$  p.u. in 0.5 s. At the same time, through phase compensation, which starts from 12 s, the phase difference between the two can be maintained near-zero within 3 s. The frequency difference between the two is always kept near zero value, this is because the grid side information is used. Thus, the capability of the SCC strategy is demonstrated.

As demonstrated in Fig. 17 that, compared with the control without any compensation, voltage amplitude compensation, and slip frequency fluctuation compensation, the proposed SCC strategy can not only restore the amplitude of stator voltage at the rated value but also minimize the envelope fluctuation of it, thus significantly improving the power quality of VSPS.

It can be seen from Fig. 18 that, compared with the results of other control strategies, the impacts (the fluctuation of voltage

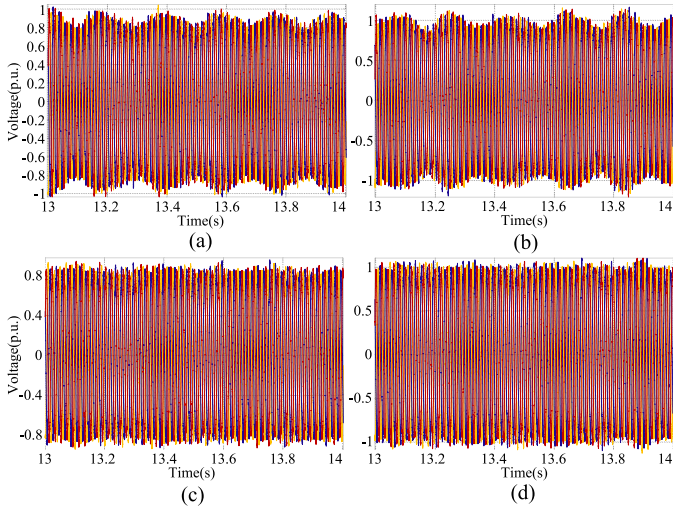


Fig. 17. Results of stator voltage before and after compensation. (a) Without compensation. (b) Amplitude compensation. (c) Slip frequency compensation. (d) SCC control.

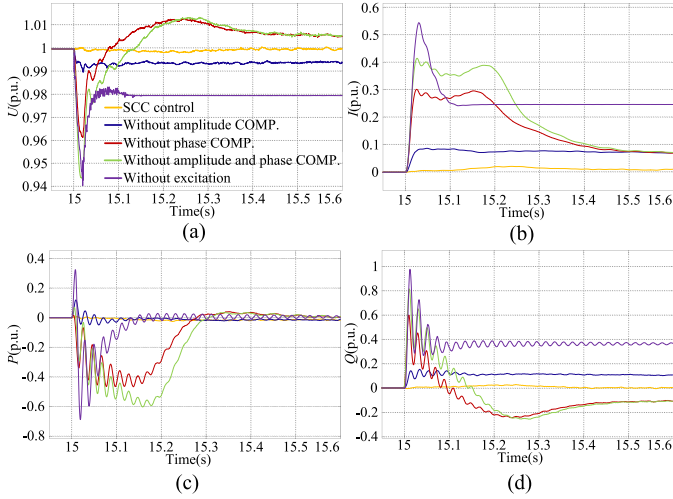


Fig. 18. Fluctuation of electric quantities in grid-connection. (a) Fluctuation of voltage. (b) Impulse of current. (c) Impulse of active power. (d) Impulse of reactive power.

and impulse of current and power) on VSPS and grid at the instant of grid-connection is minimal if applying the proposed SCC strategy. Thus, the soft cut-in control of VSPS is realized (the unit can be connected to grid without impact).

It is evident in Fig. 19 that, by adopting the traditional hard mode-switching control strategy, step mutation will occur in the control voltage and compensation voltage of the rotor-side converter. However, by applying the proposed soft mode-switching strategy, no voltage mutation will occur. It should be noted in Fig. 20 that, if the proposed soft mode-switching control of SCC strategy is adopted, the impulses of voltage, current, and power of VSPS are eliminated at the instant of switching. Thus, the superiority of the proposed strategy is verified.

As exhibited in Fig. 21 that, in the stage of load lifting, compared with traditional control methods, if the proposed

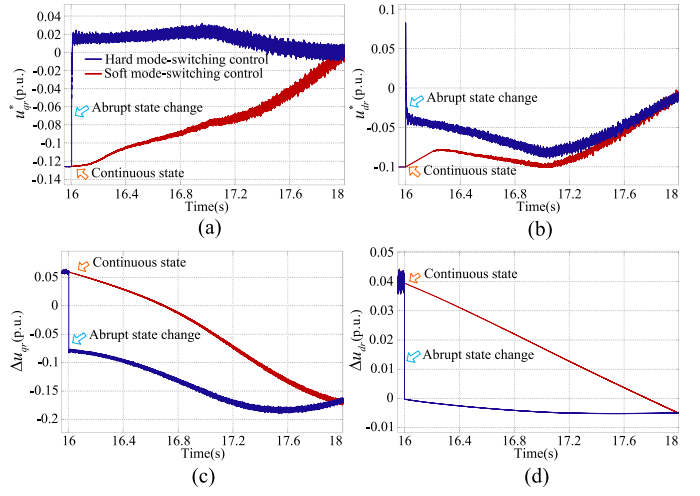


Fig. 19. Comparison of the control voltage and compensation voltage of converter between soft and hard mode-switching. (a) Control voltage of  $q$ -axis (b) Control voltage of  $d$ -axis. (c) Compensation voltage of  $q$ -axis. (d) Compensation voltage of  $d$ -axis.

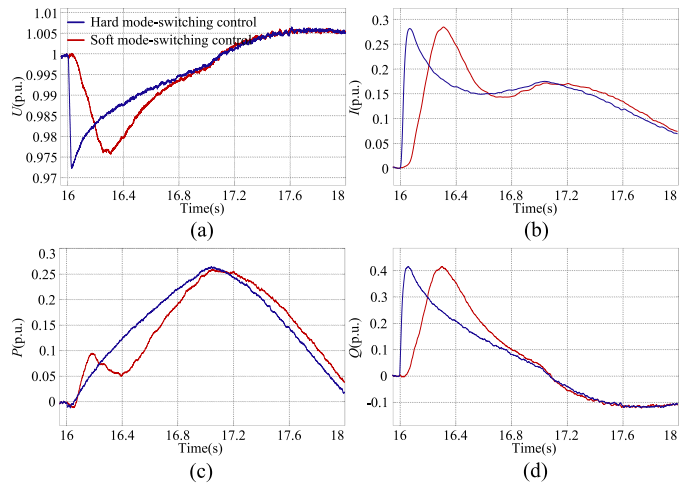


Fig. 20. Comparison of results between soft and hard mode-switching. (a) Fluctuation of voltage. (b) Fluctuation of current. (c) Fluctuation of active power. (d) Fluctuation of reactive power.

SCC strategy is adopted, the unfavorable electromagnetic torque mutation and the consequent sharp increase of GVO and sharp drop of rotor speed of VSPS are avoided. For conventional pumped storage units, it usually takes about 120 s from startup to steady-state generation mode [16]. However, it can be observed that it only takes about 50 s for VSPS. This demonstrates that VSPS is endowed with the capability of rapid mode conversion.

### B. Results of Steady-State Operation

As shown in Fig. 22 that, the simulation results are presented for the change of reference torque in the steady-state operation of VSPS. Influenced by the function of speed optimizer, this torque change leads to the rotor accelerating first and then decelerating. This is because the reference speed is changed with reference

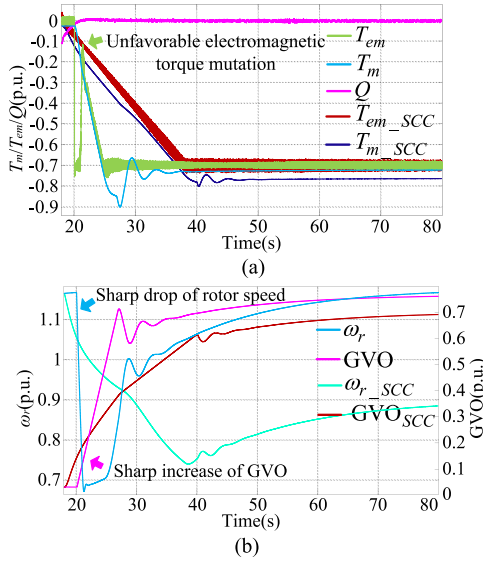


Fig. 21. Dynamic response of VSPS in the stage of load lifting. (a) Torque and reactive power. (b) Speed and GVO.

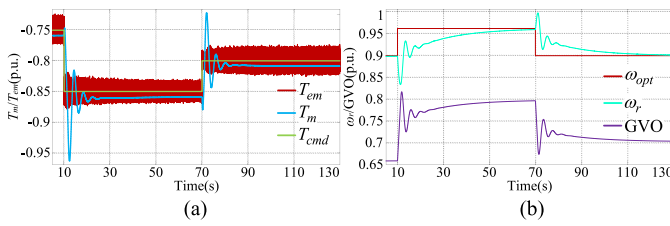


Fig. 22. Dynamic response of VSPS in steady-state operation. (a) Torque. (b) Speed and GVO.

torque. Then, the speed is slowly regulated to track the reference value by adjusting GVO and torque of RPT.

### C. Results of Cut-Out Control

As seen from Fig. 23(a) and (b) that, in the process of load rejection the speed of VSPS will increase owing to the imbalance between electromagnetic torque and mechanical torque. If traditional torque control method is employed, the electromagnetic torque and rotor speed of VSPS will oscillate, and the mechanical torque and GVO will change rapidly. However, if the SCC strategy is adopted, the unfavorable electromagnetic torque mutation and the sharp drop of GVO and sharp increase of speed are avoided. After about 20 s, GVO is gradually decreased to the no-load value. It is also evident in Fig. 23(c) and (d) that, within 20 s stator current and active power of VSPS are reduced to zero and the excitation current of the rotor is decreased to the magnetizing current.

As depicted in Fig. 24, starting at 111 s, GVO is rapidly closed and mechanical torque is correspondingly rapidly reduced to zero. If the proposed SCC strategy is adopted, with the effects of mechanical and electrical damping, the speed of VSPS can be reduced to zero in about 6 s, and at the same time, the kinetic energy of the rotor is converted into electrical energy and fed

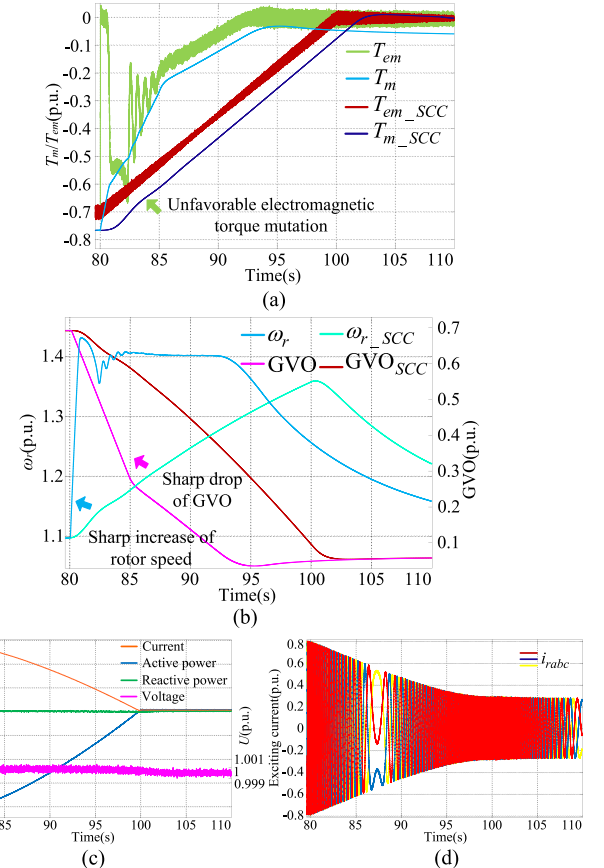


Fig. 23. Dynamic response of VSPS in the stage of load rejection. (a) Electromagnetic torque and mechanical torque. (b) Speed and GVO. (c) Electric quantities of tie-line. (d) Dynamics of excitation current.

back to the grid. However, if without SCC control, it would take 26 s to reduce the speed to zero by mechanical damping alone. Accordingly, it can be inferred that SCC control can accelerate the braking process of the unit, and can enable VSPS with the capability of the rapid shutdown.

Fig. 25 shows the whole-process simulation results of VSPS in the mode conversion under turbine working conditions. It can be seen that VSPS has successfully completed all the operating modes from startup to shut-down within 140 s, without any drastic changes of state during the process.

## VII. EXPERIMENTAL RESULTS

To test the proposed strategy experimentally, a hardware-in-the-loop (HIL) platform for VSPS which employs an OPAL-RT OP5700 simulator is built, as shown in Fig. 26. The platform consists of an electric power dispatching server, a big data storage and analysis server, a host PC, a central power controller, a back-to-back converter, and a real-time simulator, etc. The simulator is based on Intel Xeon E5 series multicore processor with 3GHz and Xilinx Virtex-7 485T onboard FPGA (minimum time step of 145 ns using eHS) with 128 channels of high-speed analog IO and 256 channels of high-speed digital IO, 16 SFP

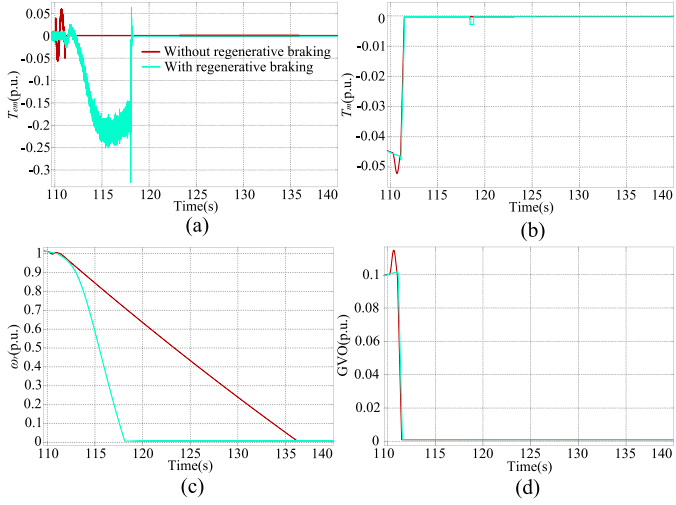


Fig. 24. Dynamic response of VSPS in disconnection with the grid. (a) Electromagnetic torque. (b) Mechanical torque. (c) Speed of rotor. (d) GVO.

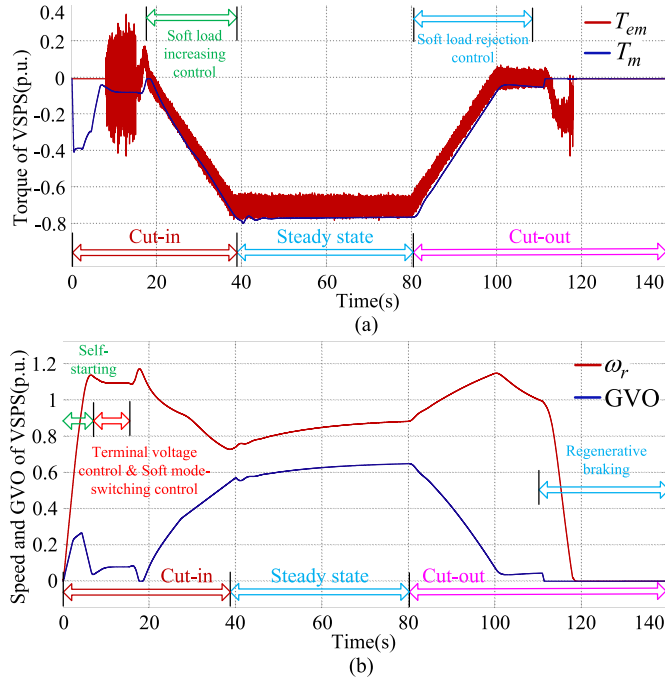


Fig. 25. Results of complete mode conversion. (a) Electromagnetic torque and mechanical torque. (b) Speed and GVO.

multimode fiber ports (adopt AURORA high-speed communication protocol with up to 5Gb/s communication speed) and LVDS synchronous cables. The experimental results are acquired by using part of the HIL equipment in the platform. On the basis of adopting RT-LAB software, and Simulink and ARTEMIS module libraries, the state space node (SSN) algorithm was used to decouple the model which was calculated in the simulator and ARTEMIS Solver was used for solution. The real-time step size of the model can be as low as  $7 \mu\text{s}$ , which ensures the real-time performance of the calculation. In the platform, the back-to-back

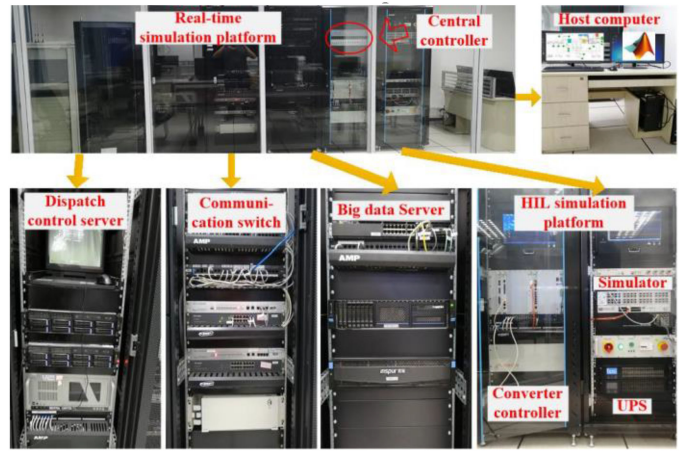


Fig. 26. HIL-based experimental platform.

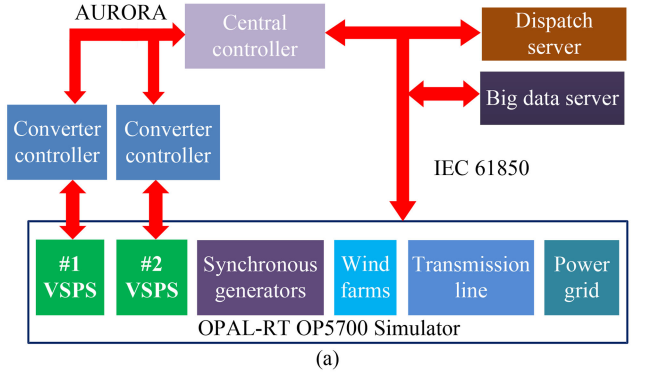


Fig. 27. Simulation model and hardware architecture of experimental platform. (a) Architecture of the experimental platform. (b) Part of the simulation model in the simulator.

converter is from SUNGROW and the control algorithm is implemented on TMS320F240 DSP from TI. The control algorithm of central power controller, which is responsible for controlling the power of converter and VSPS in real-time, is also executed in microprocessor.

As is shown in Fig. 27 that, in the experimental platform the converter control system and the central controller of VSPS, and the dispatch system and peripheral communication system are adopting the physical hardware; while the RPT, speed governor, doubly fed induction machine, and main circuit of converter for

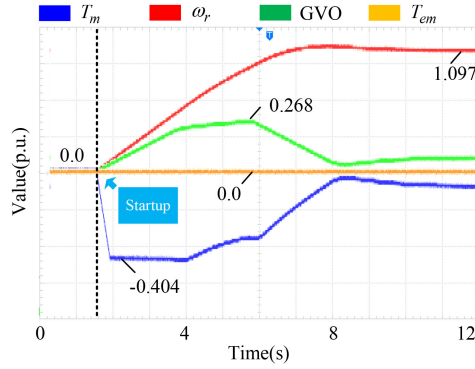


Fig. 28. Results at stage of soft self-starting.

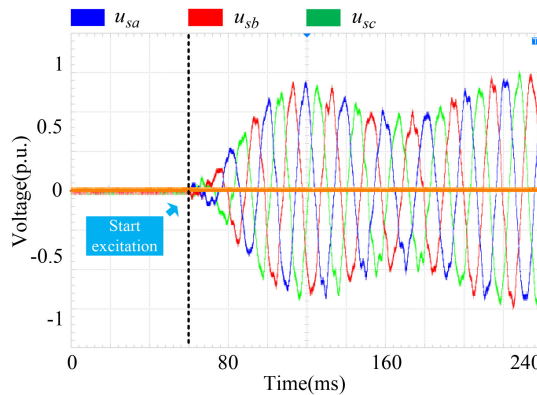


Fig. 29. Voltage of stator by EVCN control.

VSPS, and power grid, and other elements are simulated in the real-time simulator.

It can be observed in the experimental result presented in Fig. 28 that, by applying the proposed SCC strategy the rotor speed can be accelerated to the target value within 8 s. In this process, the rotor is not only accelerated rapidly but also stabilized within a short time, and the speed does not demonstrate any overshoot. It clearly shows in Fig. 29 that by using the proposed control strategy, the stator voltage is established gradually. By comparing the results of Fig. 30(a) and (b), it can be seen that the quality of voltage waveform for VSPS can obviously be improved by the proposed VCC control. When observing the difference between grid voltage and stator voltage, it can be inferred from the result demonstrated in Fig. 31 that, after employing the VCC control strategy the voltage error between grid and stator is getting smaller and smaller, which indicates that the voltage waveform of the two is becoming more and more consistent. Meanwhile, it can also be seen from the results in Fig. 32 that, after the VCC control strategy was applied, the phase difference between grid and stator was almost zero.

An interesting observation from Fig. 33 is that, through utilizing the proposed strategy the voltage, current, and power shock fluctuations of VSPS are negligible at the instant of connection. At the same time, it can be seen from Fig. 34 that the rotor excitation current can transition to the new state without dramatic change. It is especially evident by comparing the results

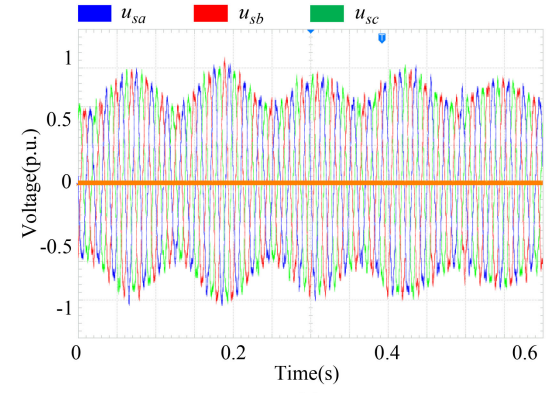


Fig. 30. Voltage of stator before and after compensation. (a) Without any compensation. (b) With VCC compensation control.

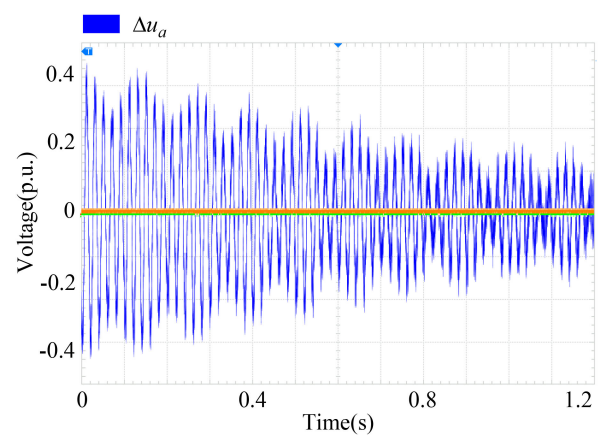


Fig. 31. Voltage error between grid and stator before connection.

exhibited in Fig. 35 that, if adopting the proposed strategy, the voltage mutations of the rotor-side converter are eliminated at the moment of the control mode switching.

Fig. 36(a) and (b) clearly shows the results of VSPS when increasing and decreasing the electromagnetic power output of it respectively. It can be seen that when the power slowly increases or decreases, the rotor speed will decrease or increase correspondingly due to the “flywheel effect” of the rotor. Due

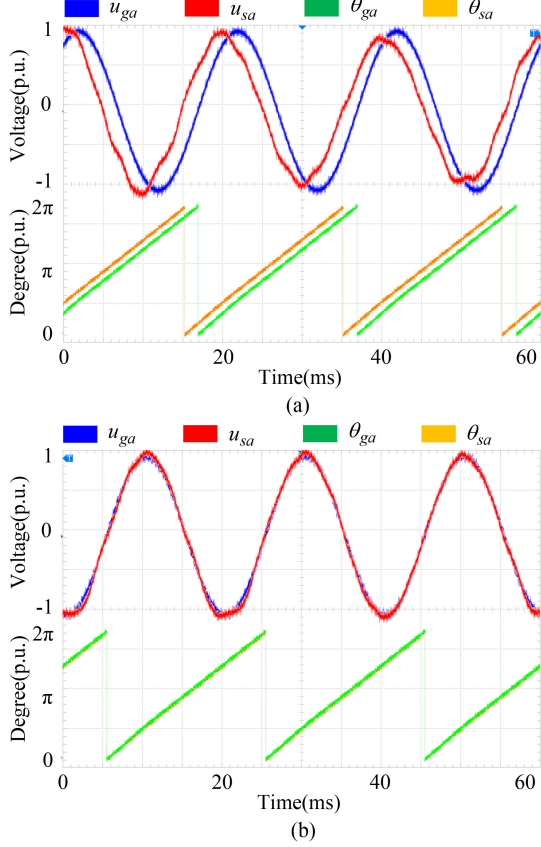


Fig. 32. Comparison of grid and stator voltage before connection. (a) Before VCC compensation control. (b) After VCC compensation control.

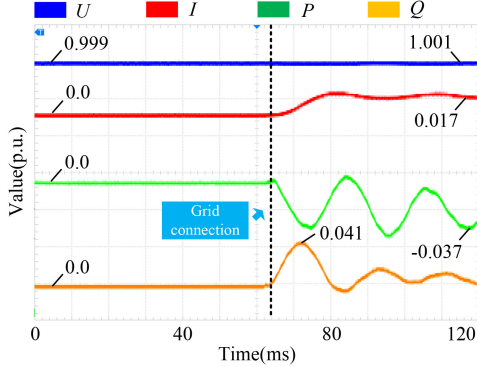


Fig. 33. Impact of voltage, current, and power at the moment of grid-connection.

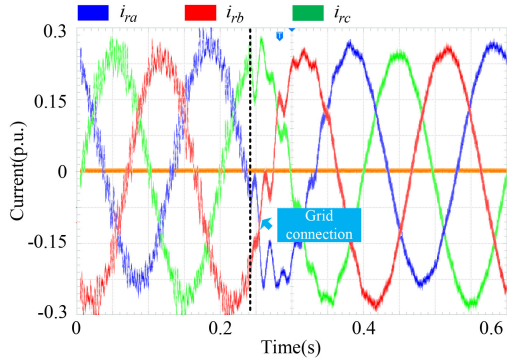


Fig. 34. Excitation current of rotor before and after grid-connection.

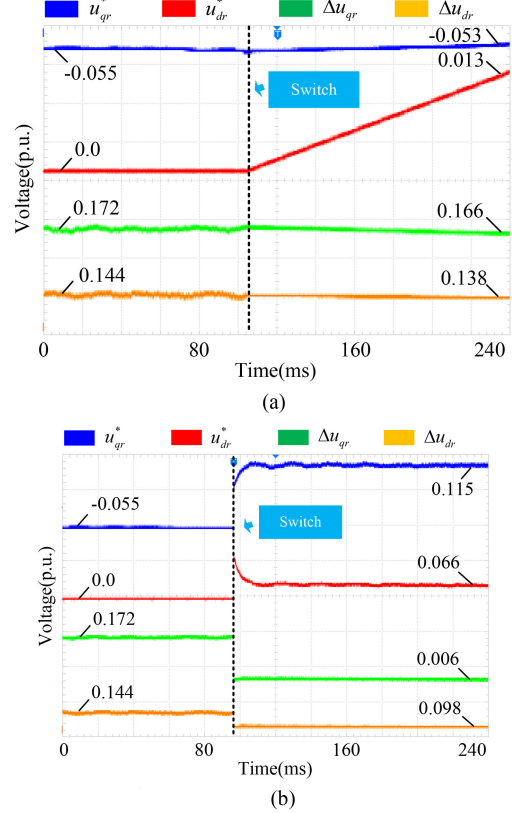


Fig. 35. Comparison of the control voltage and compensation voltage of converter between soft and hard mode-switching. (a) Results of soft mode-switching. (b) Results of hard mode-switching.

to the application of the proposed soft power control strategy, the torque, rotor speed, and GVO of the unit all change gently without spikes or oscillations.

The experimental results demonstrated above not only agree with the simulation results, but also verified the effectiveness of the proposed multistage SCC control strategy from the control results of VSPS at various stages of mode conversion.

## VIII. CONCLUSION

A multistage SCC strategy between excitation and hydraulic system has been proposed to realize the rapid, soft, and smooth mode conversion of VSPS. Several advantages can be demonstrated from the simulation and experimental results by applying the strategy. First, the controllability of the rotor is improved in the stage of the startup. The time needed for rotor speed to reach steady-state is greatly reduced while the overshoot is depressed. Second, VSPS is enabled to cut-in the grid while the speed of the rotor fluctuates, which provides the possibility for the rapid startup of it. Third, the voltage quality of VSPS is improved by the VCC in process of synchronization, and the impacts on the unit and grid are minimized at the instant of connection. Besides, the status mutation between the before and after modes is eliminated by applying the switching control function. And last, the reduction of the rotor speed is accelerated, and the

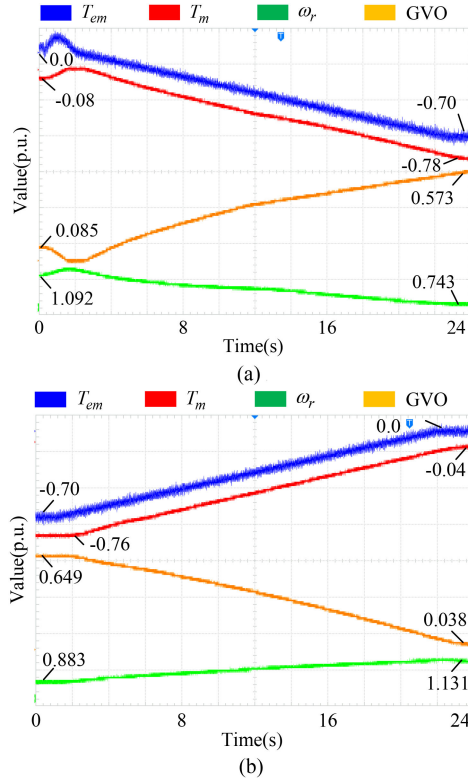


Fig. 36. Results of soft load increasing and rejection control. (a) Load increasing control. (b) Load rejection control.

rotational energy of rotor is fed back to the grid for utilization by cut-out control.

## APPENDIX

The parameters and control parameters of VSPS are shown in Tables I and II.

TABLE I  
PARAMETERS FOR BACK-TO-BACK CONVERTER OF VSPS

Item	Value	Item	Value
L	0.3	C <sub>DC</sub> (mF)	10
R	0.003	GSC PWM carrier (Hz)	2700
U <sub>DC</sub> (V)	1150	RSC PWM carrier (Hz)	1620

TABLE II  
PARAMETERS FOR GENERATOR OF VSPS

Item	Value	Item	Value
P <sub>n</sub> (MVA)	10	R <sub>r</sub> '	0.016
V <sub>s</sub> (rms)	575	L <sub>r'</sub>	0.16
V <sub>r</sub> (rms)	1975	L <sub>m</sub>	2.9
f <sub>n</sub> (Hz)	50	H <sub>g</sub> (s)	0.685
R <sub>s</sub>	0.023	F	0.01
L <sub>ls</sub>	0.18	p	3

TABLE III  
PARAMETERS FOR HYDRAULIC SYSTEM OF VSPS

Item	Value	Item	Value
k <sub>p</sub>	1.163	e <sub>gy</sub>	1.0
k <sub>i</sub>	0.105	e <sub>go</sub>	0
k <sub>d</sub>	0	e <sub>gh</sub>	0.5
T <sub>lv</sub> (s)	0.01	$\beta$	0
k <sub>a</sub>	10/3	T <sub>w</sub> (s)	0.85
t <sub>a</sub> (s)	0.07	g <sub>min</sub>	0.01
e <sub>Ty</sub>	1.0	g <sub>max</sub>	0.97518
e <sub>To</sub>	-1.0	V <sub>gmin</sub> (pu/s)	-0.1
e <sub>Th</sub>	1.5	V <sub>gmax</sub> (pu/s)	0.1

## ACKNOWLEDGMENT

The author would like to thank the Editors and Reviewers for their valuable suggestions on improving the quality of the article.

## REFERENCES

- I. Iliev, C. Trivedi, and O. Gunnar Dahlhaug, "Variable-speed operation of Francis turbines: A review of the perspectives and challenges," *Renewable Sustain. Energy Rev.*, vol. 103, pp. 109–121, 2019.
- W. Yang and J. Yang, "Advantage of variable-speed pumped storage plants for mitigating wind power variations: Integrated modelling and performance assessment," *Appl. Energy*, vol. 237, pp. 720–732, 2019.
- M. Valavi and A. Nysveen, "Variable-speed operation of hydropower plants: A look at the past, present, and future," *IEEE Ind. Appl. Mag.*, vol. 24, no. 5, pp. 18–27, Sep./Oct. 2018.
- T. Kuwabara, A. Shibuya, H. Furuta, E. Kita, and K. Mitsuhashi, "Design and dynamic response characteristics of 400 MW adjustable speed pumped storage unit for ohkawachi power station," *IEEE Trans. Energy Convers.*, vol. 11, no. 2, pp. 376–384, Jun. 1996.
- V. Koritarov *et al.*, "Modeling and analysis of value of advanced pumped storage hydropower in the U.S.," Argonne Nat. Lab., Lemont, IL, USA, Tech. Rep. ANL/DIS-14/07, Jun. 2014.
- A. Joseph, R. Selvaraj, T. R. Chelliah, and S. V. A. Sarma, "Starting and braking of a large variable speed hydrogenerating unit subjected to converter and sensor faults," *IEEE Trans. Ind. Appl.*, vol. 54, no. 4, pp. 3372–3382, Jul./Aug. 2018.
- L. Ji, Y. Shao, J. Sun, and L. Shi, "Research on self-starting strategy of variable speed pumped storage units based on model predictive control," *J. Eng.*, vol. 2017, no. 13, pp. 984–989, 2017.
- Z. Dong *et al.*, "Developing of quaternary pumped storage hydropower for dynamic studies," *IEEE Trans. Sustain. Energy*, vol. 11, no. 4, pp. 2870–2878, Oct. 2020.
- J. Lung, Y. Lu, W. Hung, and W. Kao, "Modeling and dynamic simulations of doubly fed adjustable-speed pumped storage units," *IEEE Trans. Energy Convers.*, vol. 22, no. 2, pp. 250–258, Jun. 2007.
- V. Azbe and R. Mihalic, "Transient stability of a large doubly-fed induction machine in a pumped-storage plant," *Elect. Power Syst. Res.*, vol. 142, pp. 29–35, 2017.
- M. A. Bidgoli, H. A. Mohammadpour, and S. M. T. Bathaei, "Advanced vector control design for DFIM-Based hydropower storage for fault ride-through enhancement," *IEEE Trans. Energy Convers.*, vol. 30, no. 4, pp. 1449–1459, Dec. 2015.
- R. R. Semwal, K. Desingu, T. R. Chelliah, and A. Joseph, "Two-Stage protection circuit for a multichanneled power electronic converter fed large asynchronous hydrogenerating unit," *IEEE Trans. Ind. Appl.*, vol. 55, no. 6, pp. 5947–5959, Nov./Dec. 2019.
- Y. Pannatier, B. Kawkabani, C. Nicolet, J. Simond, A. Schwery and P. Allenbach, "Investigation of control strategies for variable-speed pump-turbine units by using a simplified model of the converters," *IEEE Trans. Ind. Electron.*, vol. 57, no. 9, pp. 3039–3049, Sep. 2010.
- J. Schmidt, W. Kemmetmüller, and A. Kugi, "Modeling and static optimization of a variable speed pumped storage power plant," *Renewable Energy*, vol. 111, pp. 38–51, 2017.

- [15] J. I. Sarasúa, J. I. Pérez-Díaz, and J. R. Wilhelmi, "José Ángel sánchez-fernández, dynamic response and governor tuning of a long penstock pumped-storage hydropower plant equipped with a pump-turbine and a doubly fed induction generator," *Energy Convers. Manage.*, vol. 106, pp. 151–164, 2015.
- [16] J. Liang and R. G. Harley, "Pumped storage hydro-plant models for system transient and long-term dynamic studies," in *Proc. Power Energy Soc. Gen. Meeting*, 2010, vol. 89, no. 1, pp. 1–8.
- [17] J. Feltes *et al.*, "Testing dynamic simulation models for different types of advanced pumped storage hydro units," *Cropence*, vol. 41, no. 3, pp. 835–845, 2013.
- [18] L. Qihui, "The investigation of operation and control for a variable-speed constant-frequency wind power generation system," Ph.D. dissertation, Zhejiang Univ., 2005.
- [19] G. Tapia, G. Santamaría, M. Tellería, and A. Susperregui, "Methodology for smooth connection of doubly fed induction generators to the grid," *IEEE Trans. Energy Convers.*, vol. 24, no. 4, pp. 959–971, Dec. 2009.
- [20] N. Miller, W. Price, and J. Sanchez-Gasca, "Dynamic modeling of GE 1.5 and 3.6 wind turbine-generators," in *Proc. IEEE Power Eng. Soc. Gen. Meeting*, 2003, pp. 1977–1983.



**Yahong Chen** received the B.Sc. degree in electrical engineering and automation from Guizhou University, Guiyang, China, in 2013, the M.S. degree in electrical engineering from the Harbin Institute of Technology, Harbin, China, in 2016. He is currently working toward the Ph.D. degree in electrical engineering with Wuhan University, Wuhan, China.

His research interests include frequency and voltage control of micro-grid, modeling and control of doubly fed variable speed pumped storage unit, high performance control of brushless doubly fed variable speed pumped storage unit.



**Changhong Deng** received the B.Sc. degree from China Three Gorges University (CTGU), Yichang, China, in 1982, the M.S. and Ph.D. degrees from Wuhan University (WHU), Wuhan, China, in 1989 and 2005, respectively, all in electrical engineering.

She is currently a Professor with the School of Electrical Engineering and Automation, Wuhan University, Wuhan, China. Her research interests include security and stability analysis and control of large power grid, integration and control of renewable energy, intelligent control of power grid, optimization control of power grid, planning, modeling, and digital simulation of large power system.



**Yating Zhao** received the B.Sc. degree in electrical engineering in 2020 from Wuhan University, Wuhan, China, where she is currently working toward the M.Sc. degree in electrical engineering.